Microsc. Microanal. Microstruct. **1** (1990) 247–265 AUGUST **1990**, PAGE 247

Classification
Physics Abstracts
61.70N — 61.16D

$ErSi_2$/Si (111) interface structure determination from lattice imaging

Cécile d'Anterroches Meneau

C.N.E.T., B.P. 98, 38243 Meylan Cedex, France

(Received May 11, 1990 ; accepted December 06, 1990)

Résumé. — Dans cet article, une analyse détaillée de la structure de l'interface $ErSi_2$/Si est présentée à partir d'images obtenues en microscopie électronique en transmission haute résolution. Il est montré que dans le cas de Er Si_2, bien que ce cristal soit non centrosymétrique, certains contrastes dans l'image peuvent être prévus. L'analyse d'image révèle que deux types de structures cohabitent à l'interface $ErSi_2$/Si, qui correspondent à cet interface à des liaisons de type différent entre atomes de silicium

Abstract. — This paper is devoted to a detailed analysis of interface structure using high resolution transmission electron microscopy. In the first part the conditions needed to obtain an image similar to the projected potential are established using the dynamical theory of electron diffraction, combined with an analysis of the microscope transfer. In the second part this theory is applied to the $ErSi_2$ structure which is hexagonal and of the AlB_2 type. This case is not completely general because the approximation of the very small difference in dynamical amplitude of beams g and $-g$ applies. Thus the contrasts can be predicted. In the third part the $ErSi_2$/Si interface structure is studied. It is shown how many kinds of contrasts are required to interpret the images. The structures found correspond to two kinds of bonds for silicon atoms located at the interface plane.

1. Introduction.

It is well known that the electron wave function at the exit surface of a crystal is a linear combination of Bloch waves. These waves are submitted to a phase change by going through the objective lens. Thus the image contrast depends both on the specimen thickness and on the defocusing distance. This has been analysed in detail for semiconductors (Desseaux, Renault and Bourret, 1977). Their structure is centrosymmetric and/or the preponderant beams in the image formation, (those required to build an image of the projected potential in a first approximation) have the same behaviour. Thus there is an extended set of thicknesses and defocusing distances such that an accurate image of the crystal is obtained. A more general case will be studied in this paper and applied to the analysis of interface structures.

Interface analyses have recently been developed mainly in the field of semiconductors. In this area the most controversial interface is SiO_2/Si (d'Anterroches, 1984; Goodnick, Ferry, Wilmsen, Liliental, Fathy and Krivanek, 1985; Ourmazd, Rentschler and Bevk, 1988) because of its

dominant role in the electrical properties of MOS transistors. Using high resolution transmission electron microscopy (H.R.E.M.) the operating conditions required to obtain good images for silicon are suitable for SiO_2 which is usually amorphous. Concerning interfaces between crystallised materials two cases can occur: either they have the same structure or not.

Semiconductor multilayers belong to the first domain (Kuan and Chang, 1983; Datta, Furdyna and Gunshor, 1985). The difficulty here is to obtain a set of thickness and defocusing distance conditions (Poudoulec, Guenais, d'Anterroches and Regreny, 1989) such that the contrast in the image is different for both materials so as to emphasize the interface plane. Regarding metal over semiconductor structures, they belong to the second class (Cherns, Anstis, Hutchison and Spence, 1982; d'Anterroches, 1982); they are studied to interpret the character of the contact. In this case the difficulty, in addition to that described above is to obtain an epitaxial growth of the metal on the silicon substrate, and thus a common axis. The latter must be such that the interatomic distances in the projected lattice are not too small, given the resolution limit of the TEM used.

When these conditions are fulfilled, the interface structure is deduced from a detailed analysis of the image contrast and a comparison between micrographs and simulated images. The potential chosen to simulate the images is selected from among models established according to the geometrical theory.

This paper shows that the image contrast can be predicted for non centrosymmetric crystals under a set of conditions and put it into practice for $ErSi_2$. Moreover the detailed analysis of $ErSi_2/Si$ images shows how numerous are the informations you can deduce from defocusing series when compared to simulated images.

2. Multibeam dynamical theory.

The dynamical theory formulation is based on the motion of the electron in the potential field $V(r)$ resulting from the crystal as a whole. In this approach, the Bloch wave functions appear naturally as the steady-state solutions for $\psi(r)$, the wave function of the electron in the periodic crystal potential (Hirsch, Howie, Nicholson, Pashley and Whelan, 1965). For energies in the non-relativistic range, the steady-state wave function describing the behaviour of an electron moving in a potentiel $V(r)$ obeys Schrödinger's wave equation.

A Bloch wave function of wave vector $\mathbf{k}$ solution of the Schrödinger equation will be:

$$\Psi(r) = \sum_g C(\mathbf{k}) \exp\left(i2\pi(\mathbf{k}+\mathbf{g})\cdot\mathbf{r}\right) = \sum_g U_g \exp i2\pi\mathbf{g}\cdot\mathbf{r}$$

This is the wave function at the exist surface of the specimen. These waves are recombined by the objective lens whose defocus and spherical aberration act merely in changing the phases of the diffracted electron beams; and the image-plane wave function becomes:

$$\Psi = \sum_g U_g \exp i\left(\gamma_g + \phi_g\right) \exp i2\pi\mathbf{g}\cdot\mathbf{r} + U_0 \exp i\left(\gamma_0 + \phi_0\right) \qquad (1)$$

g are vectors of the reciprocal space, their respective dynamical amplitude and phase are U_g and γ_g according to the Howie and Whelan theory (Howie and Whelan, 1961) and ϕ_g is the phase change resulting from the objective lens spherical aberration and defocus, according to the Scherzer theory (Scherzer, 1949).

In the case of centrosymmetric crystals (Desseaux *et al.*, 1977), this summation is simplified because Friedel's law applies and $I(g) = I(-g)$.

In the case of non centrosymmetric crystals, this is more complicated. Let us consider the combination of three beams: (000) the transmitted beam and g and −g, two diffracted beams.

The contrast in the image will be given by:

$$\begin{aligned}\Psi\Psi^* = {} & U_0^2 + U_g^2 + U_{-g}^2 \\ & + 2U_0U_g \cos\,(2\pi\mathbf{g}\cdot\mathbf{r} + \phi_g - \phi_0 + \gamma_g - \gamma_0) \\ & + 2U_0U_{-g} \cos\,(2\pi\mathbf{g}\cdot\mathbf{r} + \phi_{-g} - \phi_0 + \gamma_{-g} - \gamma_0) \\ & + 2U_gU_{-g} \cos\,(4\pi\mathbf{g}\cdot\mathbf{r} + \phi_g - \phi_{-g} + \gamma_g - \gamma_{-g})\end{aligned} \tag{2}$$

The value of ϕ_g is given by:

$$\phi_g - \phi_0 = \frac{2\pi}{\lambda}\left(C_s\frac{g^4\lambda^4}{4} + \Delta f\frac{g^2\lambda^2}{2}\right) \tag{3}$$

λ is the electron wave length, and Δf the defocusing distance thus $\phi_g = \phi_{-g}$. Let us note:

$$\begin{aligned}U_{-g} &= U_g + \Delta U_g \\ \gamma_{-g} &= \gamma_g + \Delta\gamma_g\end{aligned} \tag{4}$$

First if ΔU_g is small,

$$\Delta U_g/U_g \ll 1 \tag{5}$$

the intensity becomes:

$$\Psi\Psi^* = U_0^2 + 4U_g^2A_g\cos^2\left(2\pi\mathbf{g}\cdot\mathbf{r} - \frac{\Delta\gamma_g}{2}\right) + 2U_0U_g\,(1 + A_g\cos\Delta\gamma_g)\cos 2\pi\mathbf{g}\cdot\mathbf{r}\cos\alpha_g - F_g \tag{6}$$

with:

$$\begin{aligned}\alpha_g &= \phi_g - \phi_0 + \gamma_g - \gamma_0 \\ A_g &= 1 + \frac{\Delta U_g}{U_g}\end{aligned}$$

$$F_g = +2U_0U_g\,[A_g\sin\Delta\gamma_g\sin\,(2\pi\mathbf{g}\cdot\mathbf{r} + \alpha_g) + (1 + A_g\cos\Delta\gamma_g)\sin 2\pi\mathbf{g}\cdot\mathbf{r}\sin\alpha_g]$$

Usually a structure is not given by only two beams, but by at least four, i.e. those closest to the transmitted beam. Thus let us now consider a more general case:

$$\begin{aligned}\Psi\Psi^* = {} & U_0^2 + \sum_{g\neq 0} U_g^2 \\ & + \sum_{g\neq 0} 2U_0U_g\cos\,(2\pi\mathbf{g}\cdot\mathbf{r} + \phi_g - \phi_0 + \gamma_g - \gamma_0) \\ & + \sum_{g\neq g'} 2U_gU_{g'}\cos\,(2\pi\,(\mathbf{g} + \mathbf{g}')\,\mathbf{r} + \phi_g - \phi_{g'} + \gamma_g - \gamma_{g'})\end{aligned} \tag{7}$$

Thus, if condition (5) applies, equation (6) becomes:

$$\Psi\Psi^* = U_0^2 + \sum_{g>0} 4U_g^2 A_g \cos^2\left(2\pi \mathbf{g}\cdot\mathbf{r} - \frac{\Delta\gamma_g}{2}\right) + \sum_{g>0} 2U_0 U_g\,(1 + A_g \cos\Delta\gamma_g)\,\cos 2\pi \mathbf{g}\cdot\mathbf{r}\cos\alpha_g - \sum_{g>0} F_g + \sum_{g\neq g'} F_{gg'} \tag{8}$$

One can see that the contrast is the summation of the individual contrast for each diffracted beam and a linear combination of the beams two by two corresponding to a shuffling of the image. However the shuffling term is proportional to $U_g \cdot U_{g'}$, and being equivalent in intensity to the term giving the double periodicity, it is weak in the case of weak phase object.

Thus, as in the case of centrosymmetric crystal, the term $\cos\alpha_g$ $(T(g))$ plays an important role. Then, since α_g is dependent on the thickness and the defocusing distance, the set of curves $T(g) = \pm 1$ can be plotted, on which it can be seen if there is a domain where all the curves of the same sign intersect.

An accurate reproduction of the structure will be obtained if there is a set of thickness and defocusing distance such that $\cos\alpha_g = +1$ i.e. atomic columns white (or -1 i.e.: atomic columns dark) for all the beams.

Values for U_g and γ_g have been obtained in the case of $ErSi_2$ using the multislice approximation as described below, the results are given in part 5.

3. Experimental technique.

The multislice approximation allows the wave function to be calculated at the exit surface of the specimen without solving the Schrödinger equation. It is used in the case of non perfect crystals as, in this case, it is too difficult to solve this equation for n beams, given that the degree of symmetry is decreased.

The principle of this approximation is to consider the crystal as projected on to one or several infinitely thin planes. Thus the electron wave function is submitted to a potential only in these planes. Mathematically a transmission function is applied. Between these planes over a distance Δz, the behavior of the electron wave is a propagation in vacuum. This approximation is valid if the absorption of the real crystal is not too high and if this latter can be considered as a phase object; moreover the distance Δz must be low enough to maintain a small angle scattering. This transmission-propagation sequence is repeated until the real thickness of the specimen is reached. For this work, the author run the Mc O'Keefe program.

For the simulations shown in this paper the slice thickness was chosen as half the $ErSi_2$ unit vector along the propagation axis. The phase change resulting from the phase grating was thus lower than $\pi/2$ and the change in phase between adjacent points was lower than 0.05.

The transfer of the electronic wave through the objective lens was expressed in the usual way by introducing spherical and chromatic aberrations. Furthermore the microscope characteristics were $\Delta = 9$ nm energy spread and $\alpha = 0.7$ mrad beam divergence.

The high resolution experiments were performed on a 400 kV Jeol microscope from cross-sectional specimens, obtained after mechanical polishing and Ar ion milling. The $ErSi_2$ was grown under ultra high vacuum by codepositing erbium and silicon on a Si(111) substrate followed by a high temperature in situ annealing (Arnaud d'Avitaya, Pério, Oberlin, Campidelli and Chroboczek, 1989).

Furthermore it should be mentioned that interface images are very sensitive to the microscope alignment (Meneau-d'Anterroches, 1982; Smith, Saxton, O'Keefe, Wood and Stobbs, 1983). If

the electron beam is not correctly aligned to the optical axis, it induces an artefact in the image. Roughly it acts by changing the phase of one crystal with respect to the other. Indeed the diffracted beams g_1 and g_2, for example, become $g_1+\Delta g_1$ and $g_2+\Delta g_2$; as there is no reason to have $\Delta g_1 = \Delta g_2$, the phase change is different for crystal I and crystal II. Thus their relative position in the image differs by: $n/2\pi\,(1/|\Delta g_1| - 1/|\Delta g_2|)$. Thus a translation appears which can be interpreted as a rigid body translation even though it is only an artefact.

4. $ErSi_2$ structure.

Erbium disilicide $ErSi_2$ is hexagonal and crystallizes in the AlB_2 structure; the space group is P6/mmm; the primitive cell parameters are: $c = 0.409$ nm and $a = 0.3728$ nm.

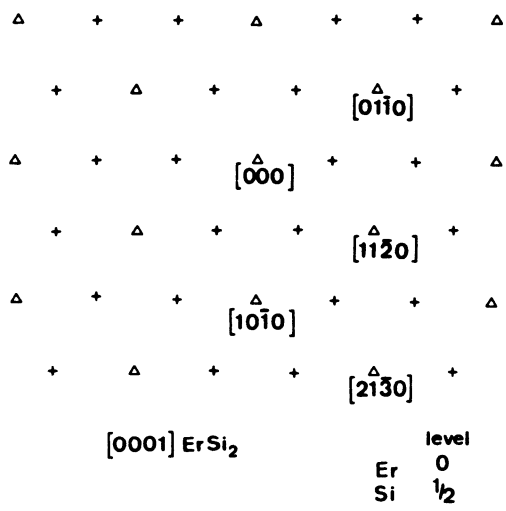

Fig. 1. — Projection of the $ErSi_2$ structure along [0001]: Δ = Er; + = Si.

The crystal is composed of two kinds of basal planes, which are silicon or erbium respectively piled up alternately. Figure 1 shows a plane view of this structure along the [0001] axis, planes $c = 0$ and $c = 1/2$ being superimposed. Each erbium atom is surrounded by 6 silicon atoms below and above. Silicon-silicon bonds are planar and thus not covalent. Let us consider the two projections which are interesting in the high resolution mode. The first, the [10$\bar{1}$0] zone axis is named A, and the corresponding projected structure is given in figure 2. The interplanar distances are: 0.205 nm (0001) planes and 0.328 nm (02$\bar{2}$0). The closest projected silicon columns are too close together to be separated given the resolution of the microscope. The second one the [12$\bar{3}$0] zone axis is named B, and its corresponding projected structure is given in figure 3. In this projection all atomic columns can be dissociated because the smaller interplanar distances are: 0.188 nm for the (2$\bar{1}\bar{1}$0) planes.

5. $ErSi_2$ simulations.

Let us now consider an $ErSi_2$ monocrystal. Running the multislice program we get the dynamical amplitude and phase for the beams playing a role in the image reconstruction. For both zone axes

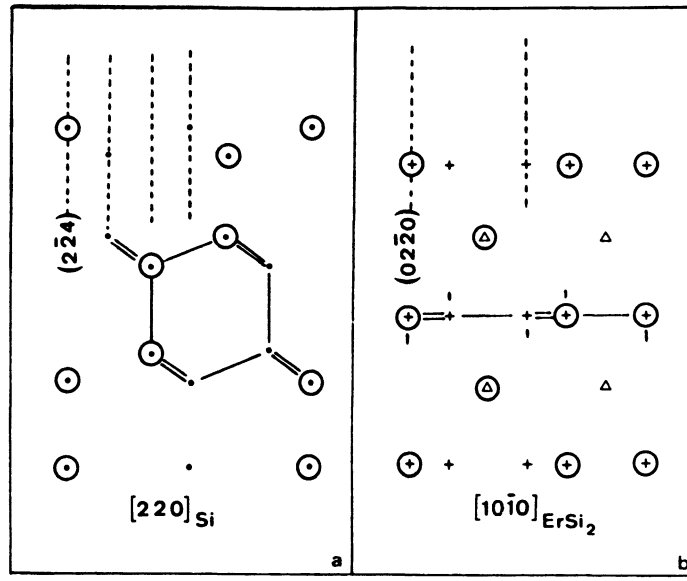

Fig. 2. — a) Projection of the Si structure along [220]. b) Projection of the $ErSi_2$ structure along [10$\bar{1}$0] encircled symbols represent atoms at level 1/2 [220] Si and [10$\bar{1}$0] $ErSi_2$ are parallel in the epitaxial relationship of the two crystals. The silicon bonds are schematically represented: (- -) bonds lying in the plane; (==) bonds running from the plane to outside.

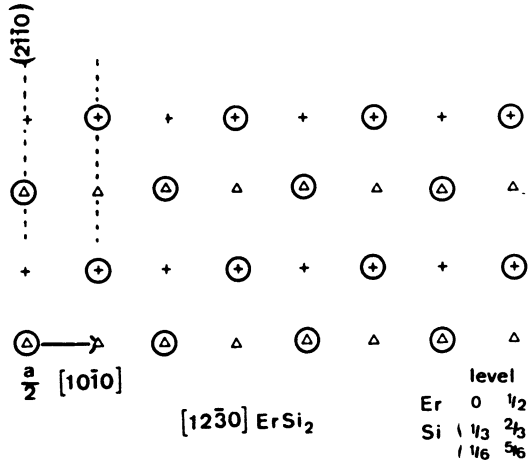

Fig. 3. — Projection of the $ErSi_2$ structure along [12$\bar{3}$0].

A and B six beams are preponderant, so the interpretation of the image contrast will be based on their behavior.

First we chose the A direction; the interesting beams are then: (0001), (0002) and (02$\bar{2}$0) (named 1, 2 and 3 respectively) and their opposites. Let us verify if approximation (6) is valid.

$\Delta U_1/U_1 = 0.003$ and $\Delta U_2/U_2$ and $\Delta U_3/U_3 < 0.001$, thus this condition applies. On the other

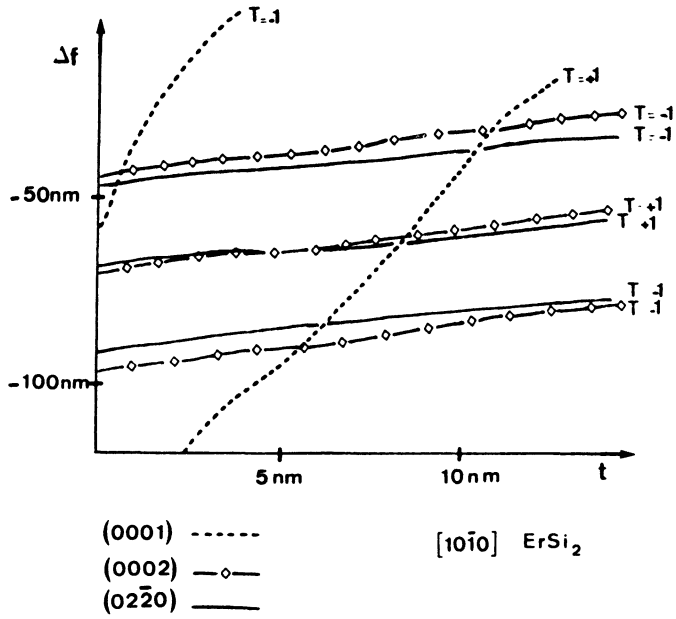

Fig. 4. — Contrast sign (T) for the six preponderant beams in the [10$\bar{1}$0] projection as a function of the defocusing distance Δf and specimen thickness t.

hand $\Delta\gamma_g$ is larger it is in the 0.06 range. The case is approximately the same for the B direction.

Then the series of curves $\cos\alpha_g = \pm 1$ (named T in the Fig.) were drawn. They are shown in figure 4. From equation (10) we deduced that an image of the projected potential of the crystal could be obtained only if $\cos\alpha_g$ is maximum or minimum for all the preponderant beams in the same defocusing distance and thickness conditions. It can be seen in the figure that the behavior is very different for each beam, and there is only one area where all are negative, i.e. in the range -53 nm $< \Delta f < -45$ nm and $t < 1.5$ nm. The corresponding simulated image (Fig. 5b) shows a contrast similar to the projected potential of the structure. This proves that while γ_g is in the 10% range the approximation $F_g \sim 0$ apply and the contrast is given by equation (8). Unfortunately this is a very small thickness and we cannot obtain a good HREM image in this case. Thus there are no conditions for obtaining an image close to the projected potential in this direction.

The projected potential is shown in figure 5a and figure 5b illustrates the simulated image closest to it, obtained for a small specimen thickness. Furthermore it can be seen that the lowest thickness, with which H.R.E.M. images can be obtained, that is 5 nm. The image closest to the negative contrast (i.e. black atomic columns) is image 5d ($\Delta f = -32$ nm). In this case the erbium columns appear grey, which is unlike the projected potential. This is due to the fact that, referring to figure 4, $T \cong 0$ for beams 1 in this area. Moreover the simulated image closest to the positive contrast (white atomic columns) is image 5e: it can be seen that although the silicon columns appear to be in position, there is a continuum for erbium. Thus there is no possibility of obtaining an image representative of the projected potential in the [10$\bar{1}$0] direction. Simulations 5c and 5f show that the image does not systematially reproduce the symmetry and the periodicity of the crystal.

In the B direction there is a little difference in the behavior of beams 2 and 3 respectively (0002) and (12$\bar{3}$0) and thus by chance there is an area well located in thickness (in the 8 nm range) where

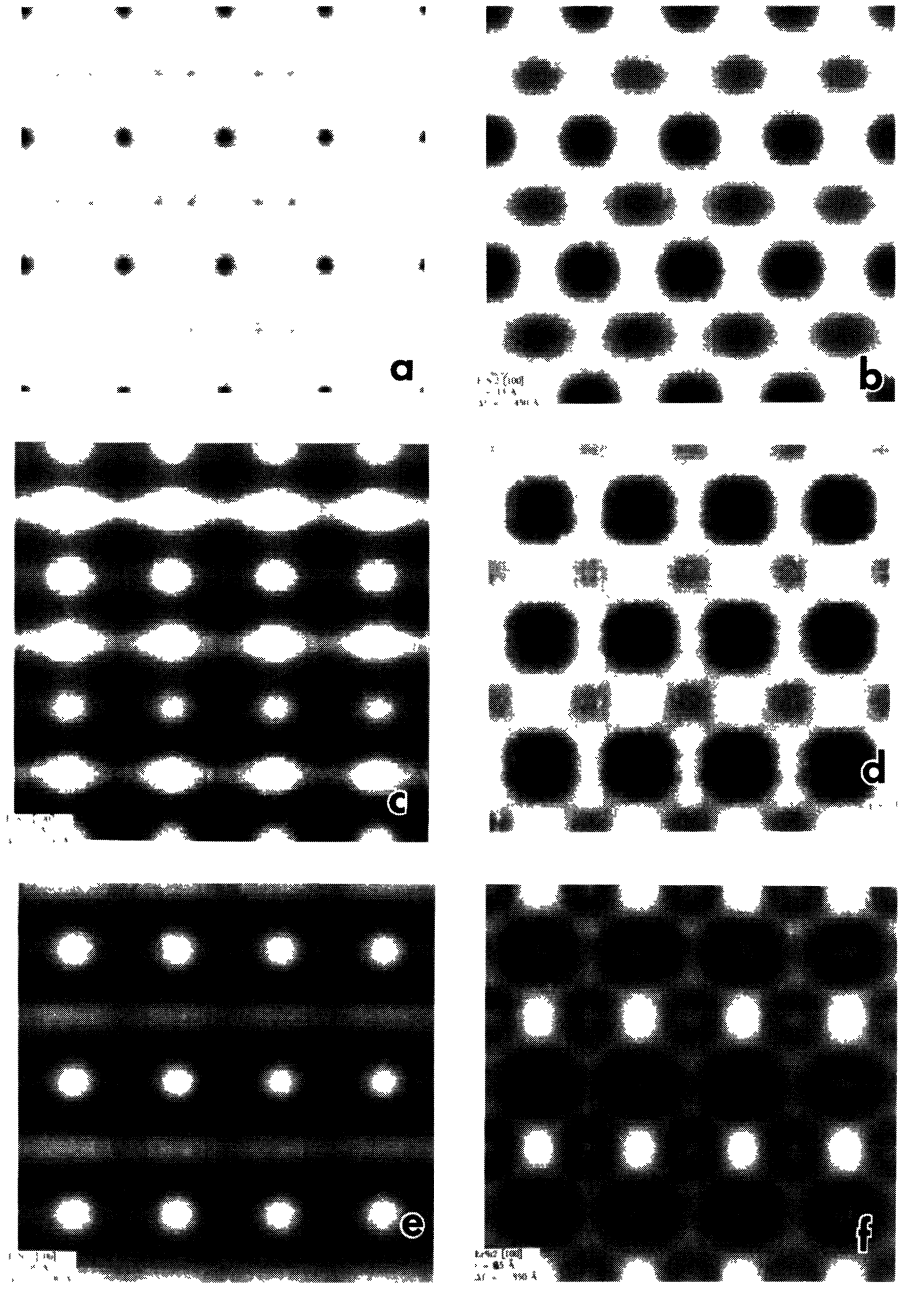

Fig. 5. — Simulated images for the projected potential a) $(ErSi_2[10\bar{1}0])$ at various sets of thicknesses t and defocusing distances Δf : b) $t = 1.3$ nm ; $\Delta f = -45$ nm. c) $t = 2$ nm ; $\Delta f = -15$ nm. d) $t = 5$ nm ; $\Delta f = -33$ nm. e) $t = 5$ nm ; $\Delta f = -10$ nm. f) $t = 8.5$ nm ; $\Delta f = -35$ nm.

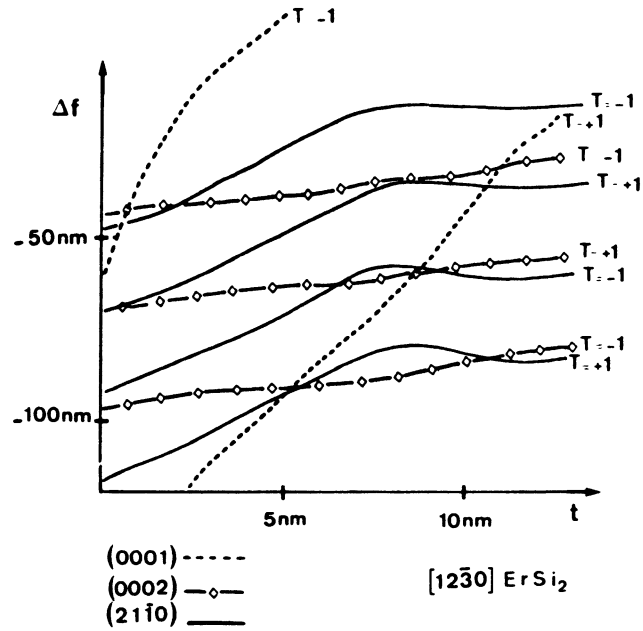

Fig. 6. — Contrast sign (T) for the six preponderant beams in the [12$\bar{3}$0] projection as a function of the defocusing distance Δf and specimen thickness t.

$T = +1$ for all the preponderant beams i.e. 1, 2 and 3 (Fig. 6). Hence for $\Delta f = -64$ nm a positive image of the projected potential in this direction can be obtained. On the other hand there are no conditions for acquiring a negative contrast, except for a specimen which is too thin or for a defocusing distance too large such that it is not possible to achieve an high resolution image. Figure 7c shows that images very far from the projected potential can be obtained and figure 7b and d show the simulations corresponding to the positive and negative contrasts respectively.

These results show that electron images of $ErSi_2$ must usually be far from the projected potential. Eventually when an image close to the projected potential can be obtained it is far from the Scherzer defocusing distance which is −40 nm according to our experimental conditions. Thus the interface structure can only be determined by comparing micrographs and simulated images. Images have to be calculated for different models, and the comparison allows a model to be determined as corresponding to the interface structure.

6. $ErSi_2$/Si interface.

Micrographs of the $ErSi_2$/Si interface have been shown in two previous papers (d'Anterroches, Perret and Brosselin, 1989; d'Anterroches, Perret, Arnaud d'Avitaya and Chroboczek, 1989). Thus this paragraph present the way to determine interface models and to choose among them this one which correspond to the interface structure.

Since the $ErSi_2$ film is completely strained coherent $ErSi_2$ and Si lattices fit well and the concept of coincidence site lattice proposed by W. Bollman (Bollman 1970) has been applied to this interface. This tool allowed its structure to be determined in unperturbed domains whose micrographs are presented in this paper. The area exhibiting interface dislocations or defects will be described in a for the coming paper.

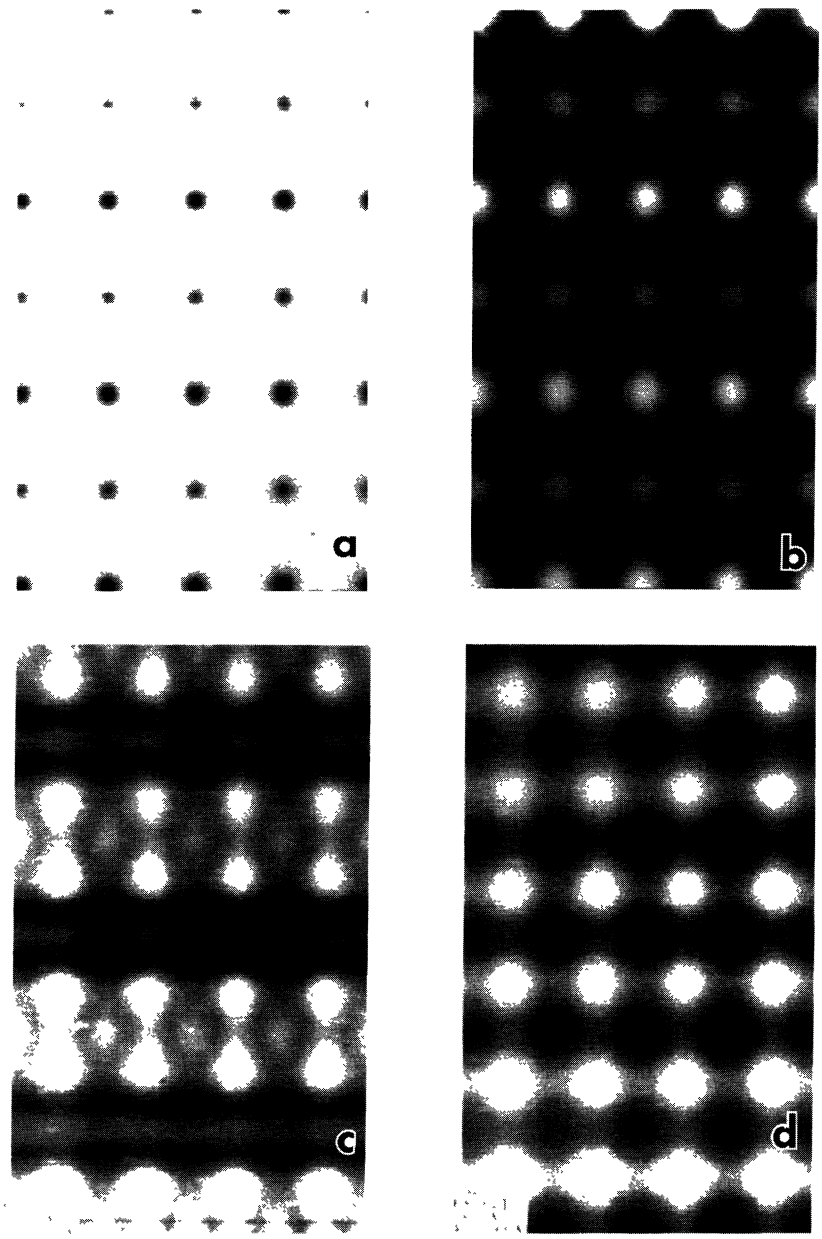

Fig. 7. — Simulated images for the projected potential a) $(ErSi_2[12\bar{3}0])$ at various sets of thicknesses (t) and defocusing distances Δf : b) $t = 4.4$ nm ; $\Delta f = -64$ nm. c) $t = 11.2$ nm ; $\Delta f = -33$ nm. d) $t = 1.7$ nm ; $\Delta f = -45$ nm.

The coincidence site lattice (CSL) is the common translations lattice. It is determined according to the following epitaxial relationship:

$$\begin{aligned}(\bar{1}11)Si \;//\; (0001)ErSi_2\\ (422)Si \;//\; (10\bar{1}0)ErSi_2\end{aligned} \qquad (9)$$

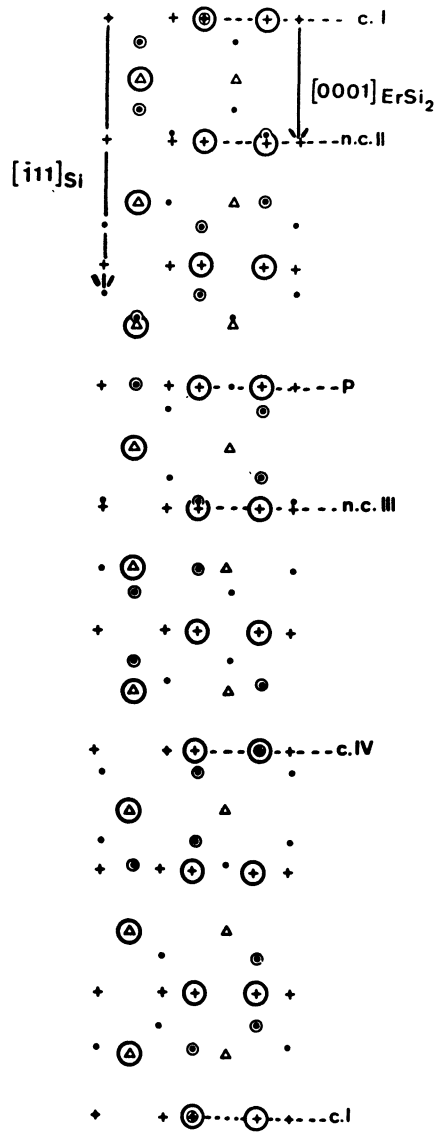

Fig. 8. — Co-set I for the CSL obtained from the epitaxial relationship (1) along the $[10\bar{1}0]$ projection. Possible interface planes corresponding to coincidences I, II, III and IV are underlined. It is shown that common planes such as P are not systematically filled by atoms in coincidence. • = Si_S; + = Si_e; △ = Er encircled symboles correspond to atoms at level 1/2.

Having $ErSi_2$ as reference the unit cell of the CSL is:

$$9[0001],\ [21\bar{3}0] \text{ and } [01\bar{1}0]; \tag{10}$$

and in the Si crystal it is:

$$4[\bar{1}11],\ 1/2[211] \text{ and } [02\bar{2}] \tag{11}$$

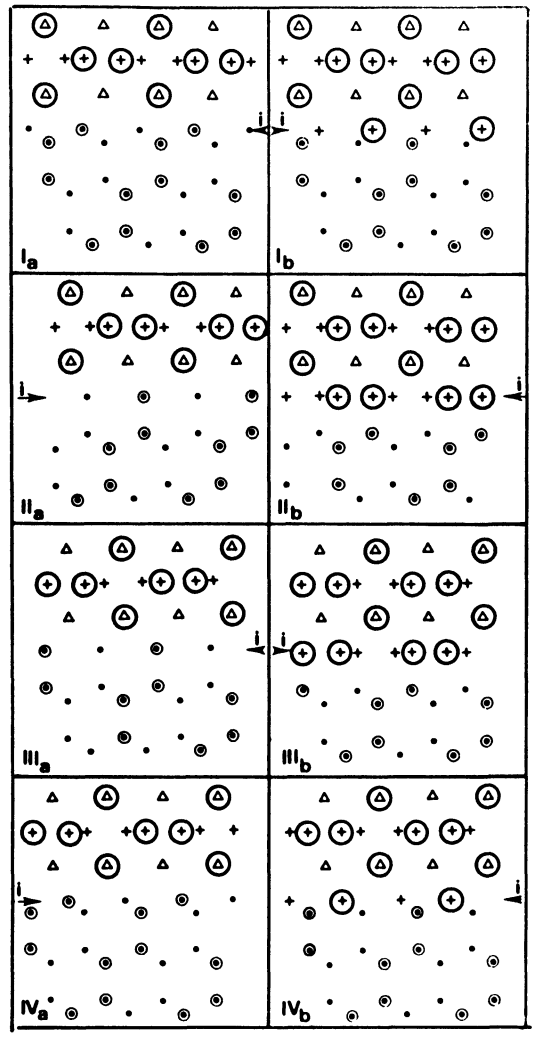

Fig. 9. — 8 models for the interface structure deduced from the 4 co-sets corresponding to the ($ErSi_2$, Si) CSL.

A CSL is independent of atomic position. The problem is then to determine all the interfaces maintening the CSL invariant, by finding all the possible origins of the CSL, and therefore settling the corresponding co-sets (d'Anterroches and Bourret 1984).

Si and $ErSi_2$ structures may be described as the superposition of atomic lattices, the nodes of which are occupied by equivalent atoms. According to D. Gratias's definition (Gratias, Portier, Fayard and Guymont, 1979) a sublattice is a subset from among the Wyckoff positions involved and which shows a translation group; silicon and $ErSi_2$ will be described this way.

Silicon has a diamond structure. The corresponding space group is Fd3m and the silicon atoms are in positions 8(a) 0,0,0 and 1/4, 1/4, 1/4 + c.f.c. according to the International Tables of X-ray crystallography (1969). Hence the silicon atoms form two partial atomic sublattices translated from each other by 1/4, 1/4, 1/4.

Erbium disilicide has a AlB_2 structure. The corresponding space group is $P6/_{m\,m\,m}$ in which erbium atoms are in position 1(a), 0,0,0, and silicon atoms are in positions 2(d) 1/3, 2/3, 1/2 and

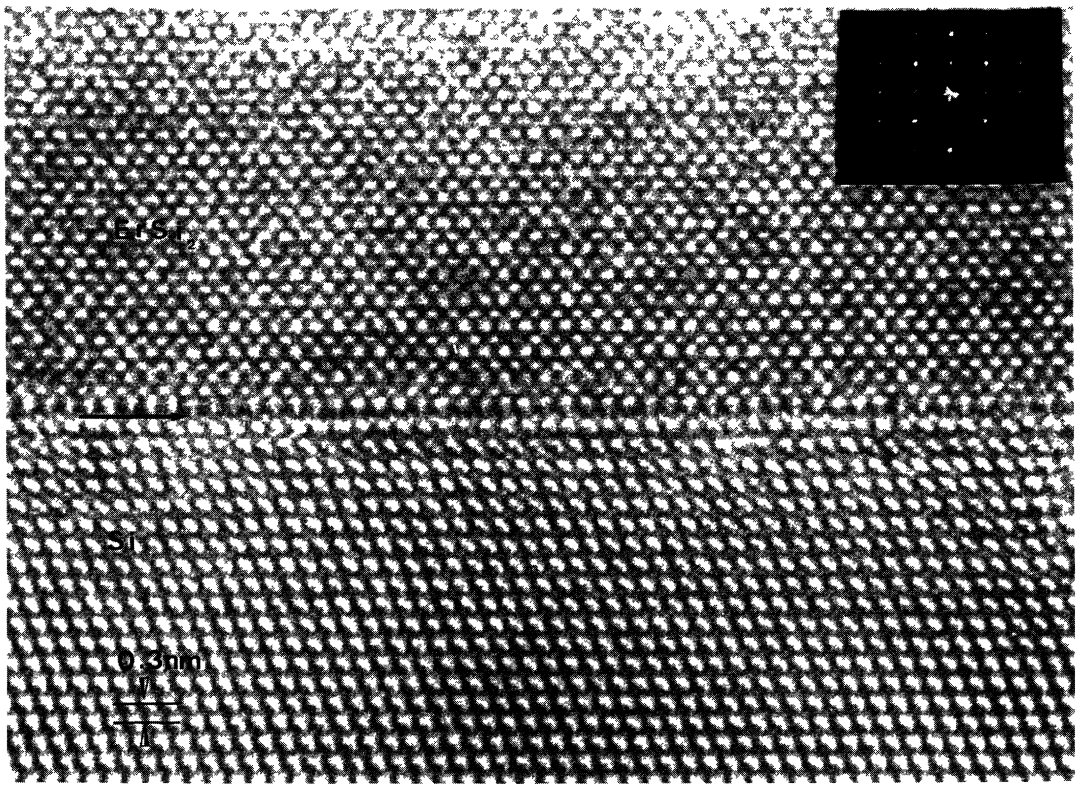

Fig. 10. — HREM image of the interface $t = 5$ nm; $\Delta f = -10$ nm along the [1010] axis. The interface plane is accurately located.

2/3, 1/3, 1/2. Thus the erbium atoms form one total atomic sublattice, while the silicon atoms form two partial atomic sublattices translatted from each other by 1/3, - 1/3, 0.

This description shows that four equivalent cosets can account for the above CSL. The origin of the co-sets is respectively Si_s 0,0,0 in coincidence with Si_e 1/3, 2/3, 1/2 or 2/3, 1/3, 1/2, and Si_s 1/4, 1/4, 1/4 in coincidence with Si_e 1/3, 2/3, 1/2 or 2/3, 1/3, 1/2 (Si_s belongs to bulk silicon while Si_e belongs to bulk $ErSi_2$).

The co-set presented in figure 8 corresponds to Si_s 0,0,0 in coincidence with Si_e 1/3, 2/3, 1/2. What is remarkable is that four planes contain silicon atomic sites in coincidence or in near coincidence, and these four planes present the four possible coincidences. Thus the four co-sets are merely described is this figure. The only difference is for planes II and III where the atomic positions are in near coincidence, but this is not important for the following demonstration.

The silicon environment in bulk silicon is completely different from what it is in $ErSi_2$. The bond angles and distances vary from 109° to 120° and 0.235 nm to 0.218 nm. Thus from these four planes 8 models for the interface structure can be proposed: the so-called models (a) when the atomic positions of bulk silicon are maintained at the interface, and models (b) when the atomic positions of silicon in bulk $ErSi_2$ are maintained. These models are presented in figure 9.

Among the models proposed someones do not represent exactly the $ErSi_2$ or the Si structure at the interface. Indeed the selected atomic position have been chosen according to two conditions:

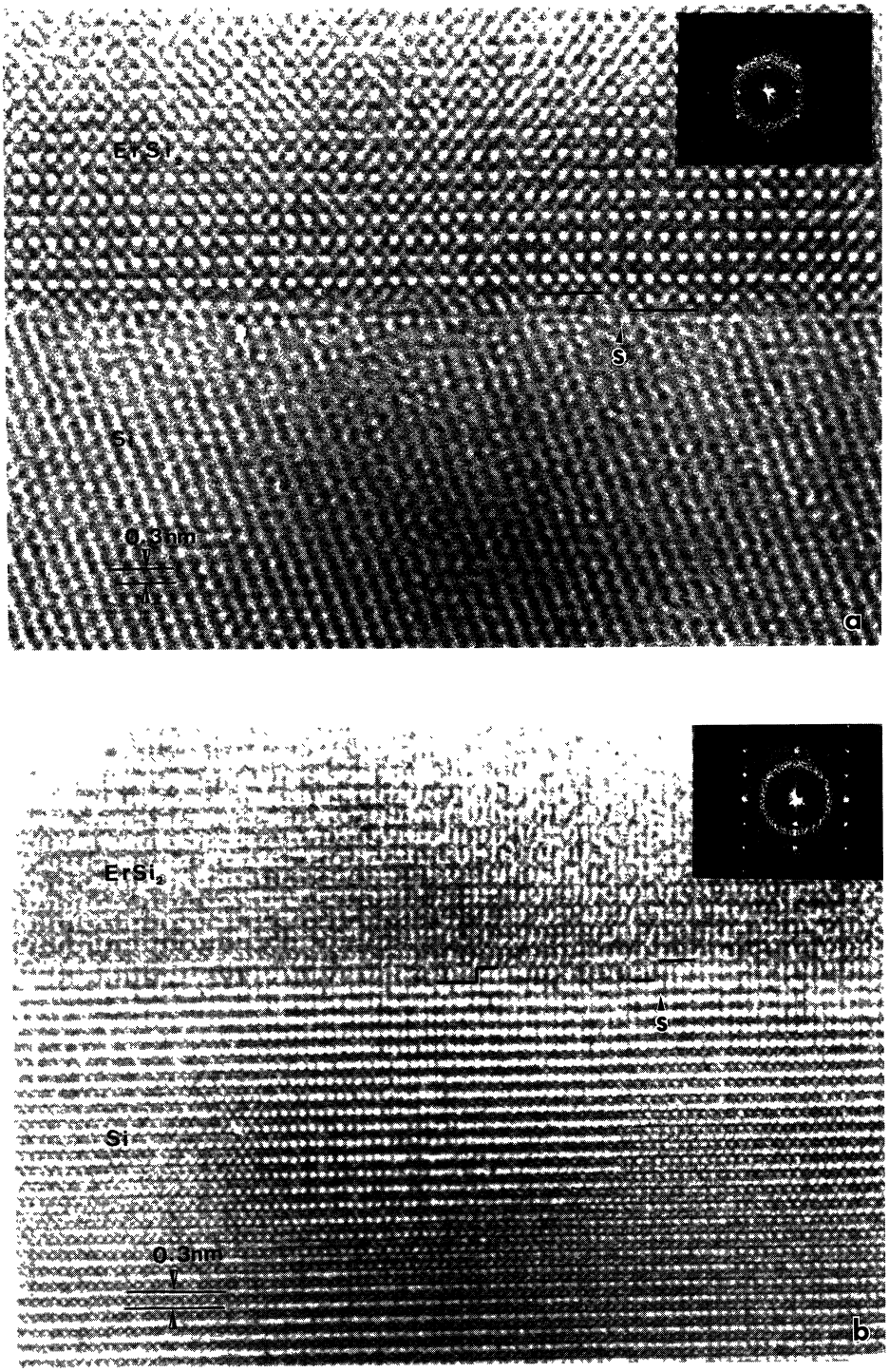

Fig. 11. — HREM image of the interface showing that steps one atomic plane high are present at the interface. a) Projection along the [1010] axis $\Delta f = -21$ nm. b) Shows clearly that there is no associated dislocation, projection along the [1230] axis, $\Delta f = -7$ nm.

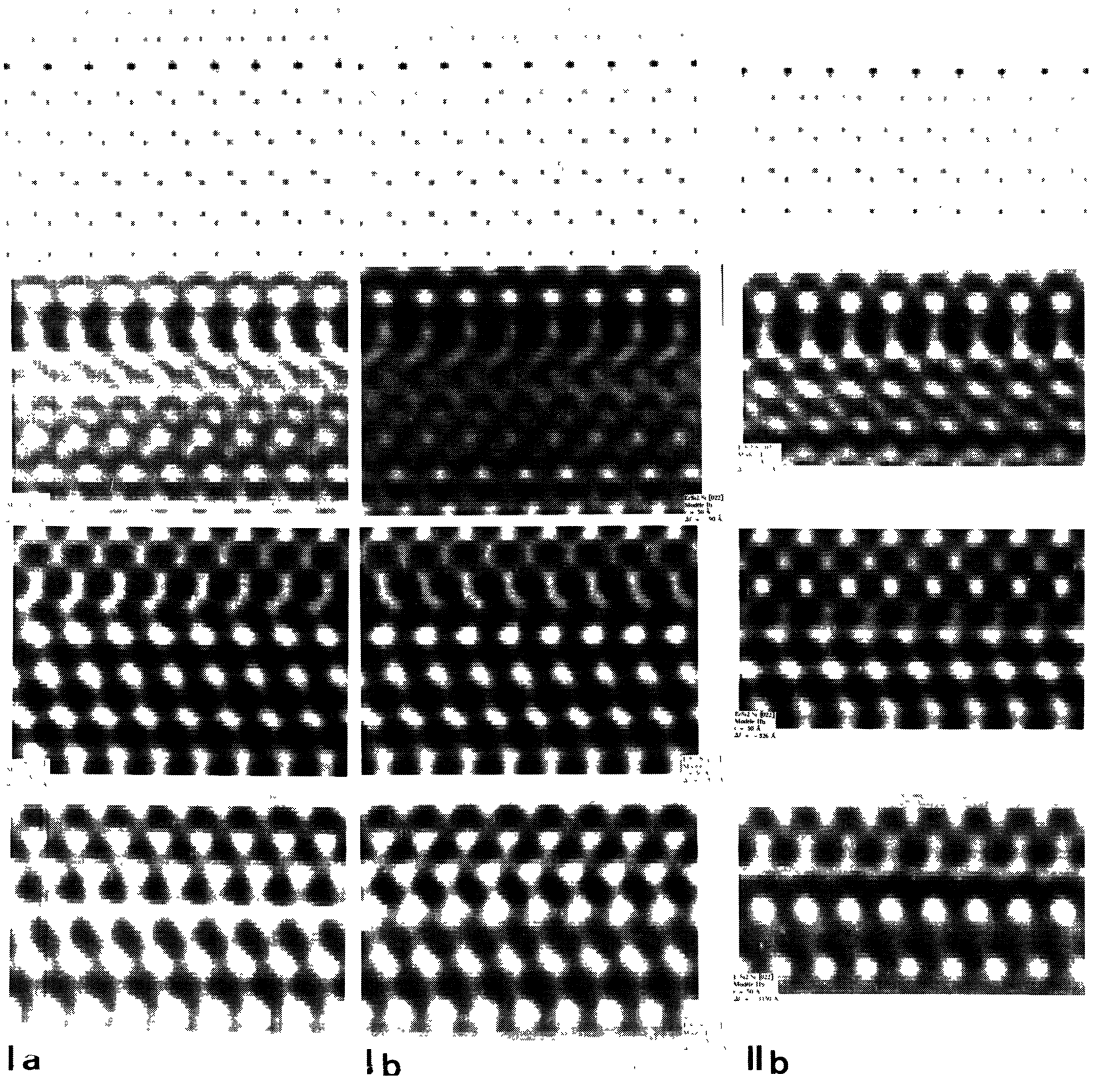

Fig. 12. — Image simulation for the three possible interface structures. For each the projected potential is given as well as a defocusing serie: $\Delta f = -9$ nm; -33 nm; -110 nm. And $t = 5$ nm.

first the interatomic distances must be as close as possible to their value in bulk crystals. Secondly there must be a minimum number of dangling bonds. No solution has been found to apply these two conditions to two models: models IIa and IIIa. Hence they have to be eliminated.

Taking into account the relative positions of the two crystals, it has been shown that models III and IV do not apply to the HREM images obtained. However, they do not have to be completely eliminated. In fact they are related to models I and II by a 180° rotation about the [111] Si axis. This is a kind of twin relation; a number of authors (Tung, Gibson and Poate 1983, Bennett, Johnson and Halawith 1988) have already shown that such a relation occures in the $NiSi_2/Si$ system depending on the film thickness. Thus, even if it is not the case in the present work, a set of growth

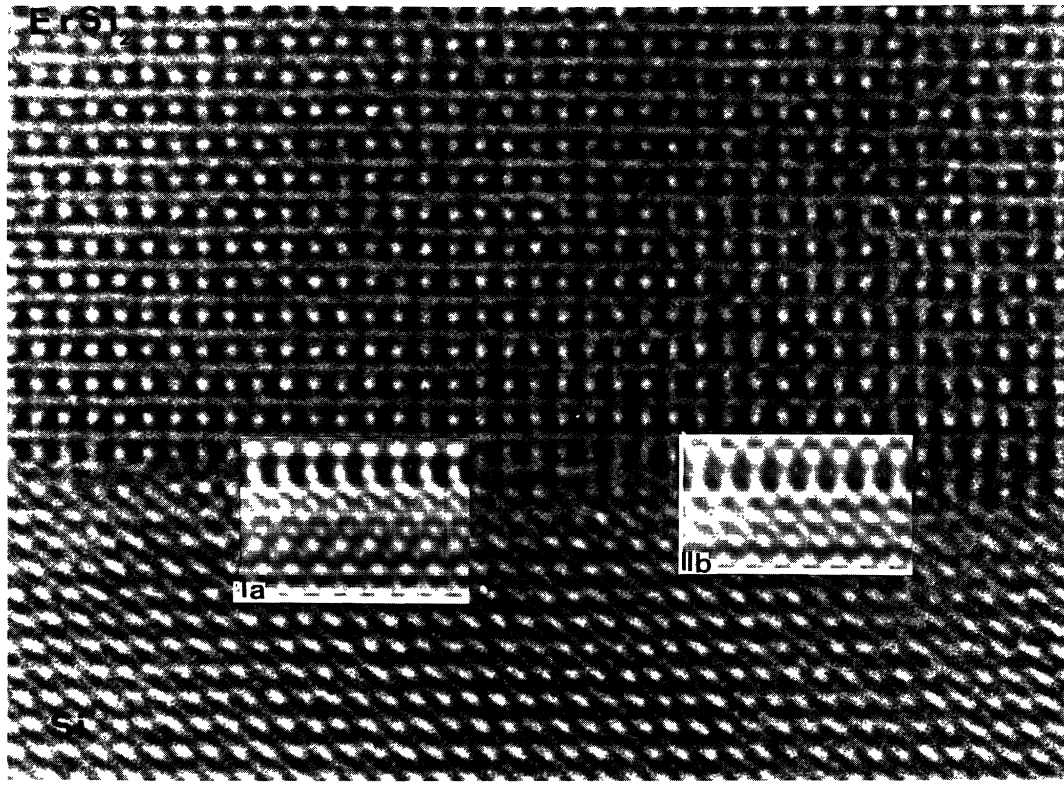

Fig. 13. — Comparison between HREM image and simulations $\Delta f = -9$ nm. $t = 5$ nm. It is difficult to determine if model I or II apply. At this defocusing distance the superimposition of the two interface structures blurces the image contrast.

or thickness conditions may be found to obtain this structure.

The reasons why models I and II apply are given below.

From the image obtained at $\Delta f = -100$ nm, figure 10, the interface plane is detectable without ambiguity, then, from the measurement of the relative position of $ErSi_2$ and Si, we deduce that it is a type I plane. However on the co-set (Fig. 8), it can be seen that a step [0001] $ErSi_2$ at the interface, without associated dislocation but only a 0.07 c [0001] rigid body translation, allows the passage from plane I to II. The images shown in figure 11 show such steps parallele to the [110] direction (Fig. 11a) or perpendicular to this direction (Fig. 11b). Thus interfaces planes I and II are present.

This result is very important as far as the electrical properties of the interface are concerned. Indeed Si orbitals and dangling bonds are not the same for interfaces I or II, thus the reference level is not the same and as a result there is a difference in the Schottky barrier heights (Lefebure, Lannoo, Priester, Allan and Delerue, 1987).

Image simulations have been calculated for models Ia, Ib and IIb at a number of defocusing distances. Those chosen in figure 12 show that the image closest to the projected potential is the image for which the two different models present the strongest difference.

The comparison between micrographs and simulated images shows that there are defocusing

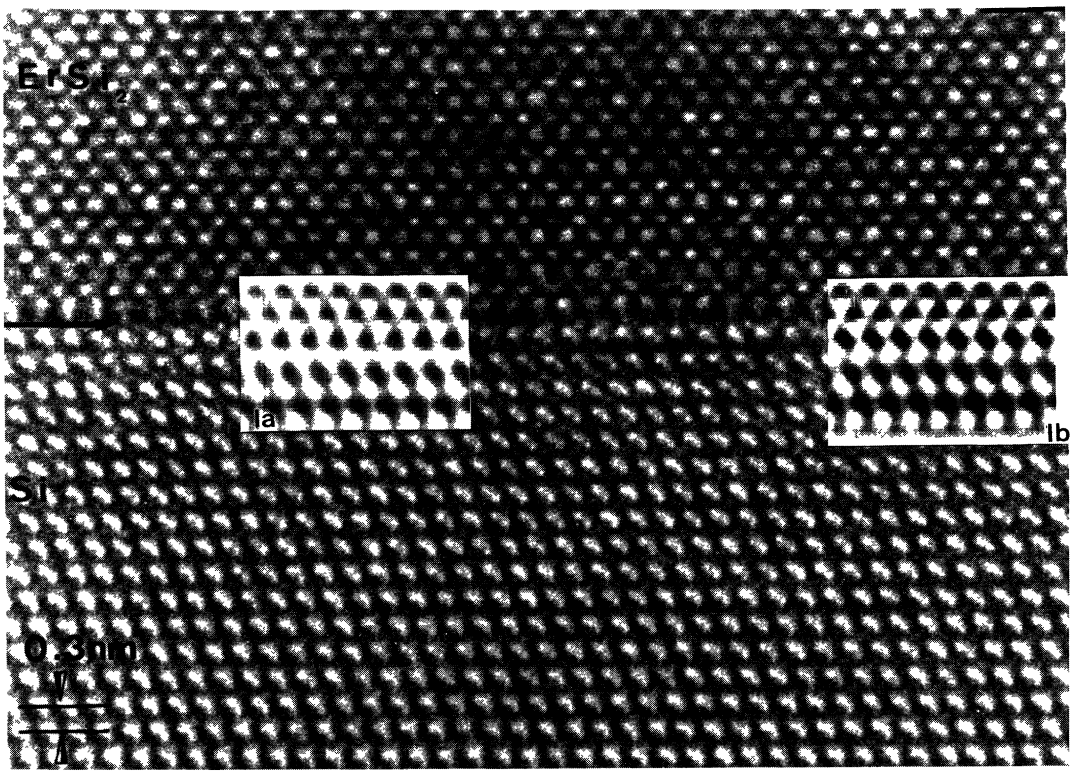

Fig. 14. — Comparison between HREM image and simulations. $\Delta f = -110$ nm. $t = 5$ nm. It is difficult to determine if model Ia or Ib apply. The difference in contrast between these two models is too slight at this defocusing distance.

distances such that the contrast is very sensitive to the structure variation. In terms of structure variation we are talking about the fact that steps at the interface, perpendicular to the zone axis, imply that the projection we obtain in the image is the superimposition of interface I and interface II.

For example the comparison between image and simulation at $\Delta f = -9$ nm shown in figure 13, prove that for this defocusing distance it is difficult to determine if model I or model II applies. Another difficulty is to choose between models Ia and Ib at $\Delta f = -110$ nm, figure 14. Indeed the differences are represented by only a slight change in the dots orientation which is not obvious. Fortunatly there is at $\Delta f = -33$ nm (Fig. 15) a contrast at the interface which differs highly for models Ia and Ib and the comparison with micrographs shows clearly that model Ia only applies. This defocusing distance seems to be the least sensitive to the structure superimposition.

7. Conclusion.

It has been shown in this paper that the conditions for obtaining in the high resolution mode, an image which is directly interpretable as the projection of the crystal structure, can be achieved in the case of non centrosymmetric crystals if the phase shift between g and $-g$ is in the 10% range.

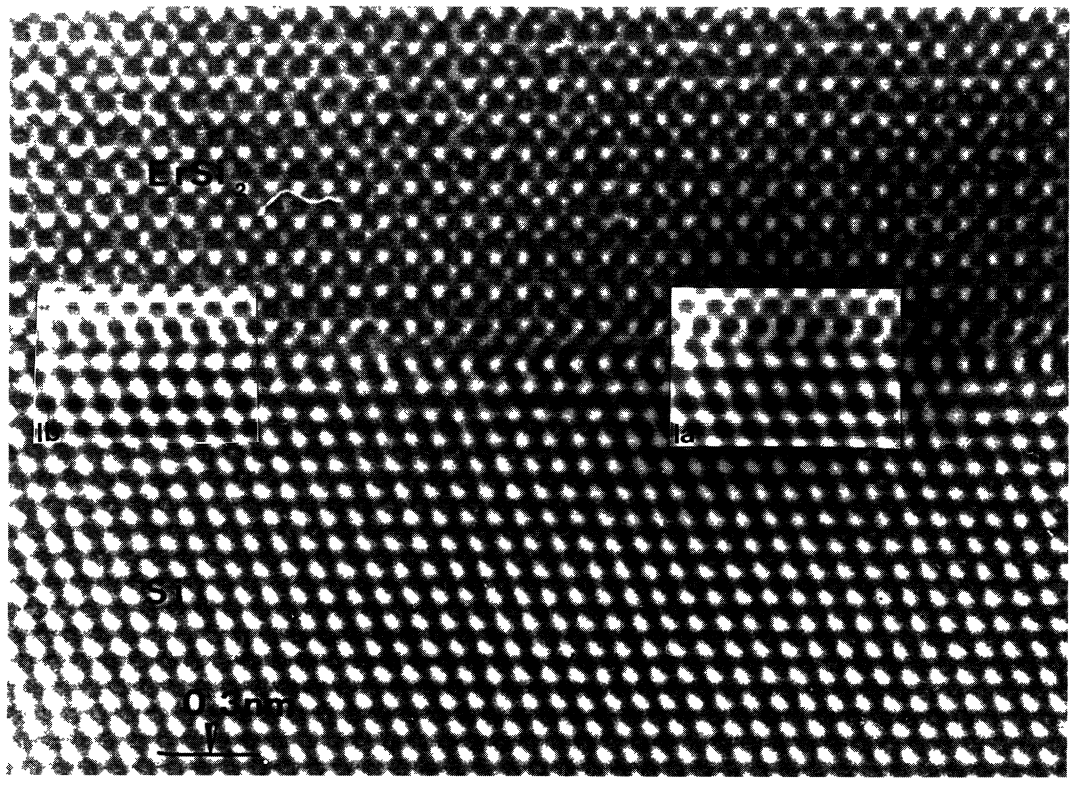

Fig. 15. — This comparison between HREM image and simulation at $\Delta f = -33$ nm $t = 5$ nm clearly reveals that only model Ia applies. This defocusing distance is such that the image contrast is less sensitive to the interface structure superimposition.

However the defocusing distance can be far from the Scherzer value.

It has been shown for example that if $ErSi_2$ is observed along the $[10\bar{1}0]$ direction there are no conditions for obtaining an image of the projected potential in the positive contrast (that is, white atomic columns), and if it is observed along the $[12\bar{3}0]$ direction, there are no conditions for obtaining it in the negative contrast.

Despite this fact, images taken at various defocusing distances are rich in information. It has been shown that, when the contrast is very different for both crystals the interface plane can be very well localised and the C.S.L. plane corresponding to the interface plane can be determined. Moreover, if the contrast is blurred for one crystal, steps at the interface are revealed. Finally, if thickness and defocusing distance are accurately measured, a comparison between simulated images and micrographs allows the interface structure to be determined.

It has thus been demonstrated that the $ErSi_2/Si$ interface structure is a combination of two structures whose main difference is in the atoms which are located at the interface plane. Indeed in structure Ia the silicon atoms are in the position they are in bulk silicon, and in structure IIb, the interface silicon atoms are in the position they are in bulk $ErSi_2$. As the electron band structure of silicon is different in both cases, the electrical properties of this interface must be a combination of both. This result prove the importance of a detailed and precise interpretation of micrographs in order to determine interface structures.

References

ARNAUD d'AVITAYA F., PERIO A., OBERLIN J.C., CAMPIDELLI Y. and CHROBOCZEK J.A., *Appl. Phys. Lett.* **54** (1989) 2198.
BENNETT P.A., JOHNSON A.P. and HALAWITH B.N., *Phys. Rev. B.* **37** (1988) 4268.
BOLLMAN W., Crystal defects and crystalline interfaces (Springer-Verlag) 1970.
CHERNS D., ANSTIS G.R., HUTCHISON J.L. and SPENCE J.C.H., *Philos. Mag. A* **46** (1982) 849.
d'ANTERROCHES C., *Surf. Sci.* **168** (1982) 751.
d'ANTERROCHES C., *J. Microsc. Spectrosc. Electron.* **9** (1984) 147.
d'ANTERROCHES C. and BOURRET A., *Philos. Mag. A* **49** (1984) 783.
d'ANTERROCHES C., PERRET P., ARNAUD d'AVITAYA F. and CHROBOCZEK J.A., Proceedings EMRS (Strasbourg, 30 May 1989) 1989.
d'ANTERROCHES C., PERRET P. and BROSSELIN J.R., International Congress on Intergranular and Interphase Boundaries in Materials, *J. Phys. Colloq. France* **50** (1990) C1-
DATTA S., FURDYNA J.K. and GUNSHOR R.L., *Superlattices and Micros.* **1** (1985) 327.
DESSEAUX J., RENAULT A. and BOURRET A., *Philos. Mag.* **35** (1977) 357.
GOODNICK J.M., FERRY D.K., WILMSEN C.W., LILIENTAL Z., FATHY D. and KRIVANEK O.L., *Phys. Rev. B* **32** (1985) 8171.
GRATIAS D., PORTIER R., FAYARD M. and GUYMONT M., *Acta Cryst.* **AB5** (1979) 885.
HIRSCH P., HOWIE A., NICHOLSON R.B., PASHLEY D.W. and WHELAN M.J., Electron Microscopy of thin crystals (R.E. Krieger publishing co.) 1965.
HOWIE A. and WHELAN M.J., *Proc. Roy. Soc. A* **263** (1961) 217.
KUAN T.S. and CHANG C.A., *J. Appl. Phys.* **54** (1983) 4408.
LEFEBURE I., LANNOO M., PRIESTER C., ALLAN G. and DELERUE C., *Phys. Rev. B* **36** (1987) 1336.
MENEAU-d'ANTERROCHES C., Thèse de doctorat d'Etat, Grenoble (1982).
OURMAZD A., RENTSCHLER J.A. and BEVK J., *Appl. Phys. Lett.* **53** (1988) 743.
POUDOULEC A., GUENAIS B., d'ANTERROCHES C. and REGRENY A., *J. Cryst. Growth* **100** (1989) 529.
SCHERZER O. *J. Appl. Phys.* **20** (1949) 20.
SMITH D.J., SAXTON W.O., O'KEEFE M.A., WOOD G.J. and STOBBS W.M., *Ultramicroscopy* **11** (1983) 263.
TUNG R.T., GIBSON J.M. and POATE J.M., *Appl. Phys. Lett.* **42** (1983) 888.